Electronic Supplementary Information

Robust and Superwetting Island-shaped Phytate Bimetallic Oxyhydroxide Porous Nanoclusters via a Mild Self-assembly—Etching-catching—Electrochemical Oxidization Strategy for Enhanced Oxygen Evolution Reaction

Yanqing Wang[a], Yuemeng Li[a], Liping Ding[b,c], Xi Xu[a], Zhe Chen[a], Chaojiang Li[a], Jun Ding[a,*]

a Department of Materials Science & Engineering, National University of Singapore, 117575, Singapore

b Department of Chemical and Biomolecular Engineering, National University of Singapore, 117576, Singapore

c School of Chemistry and Chemical Engineering, Nantong University, Nantong 226007, China

Experimental Section

Materials

Ni foam(NF) was purchased from Latech Scientific Supply Pte. Ltd. Phytic acid(PA), $FeCl_3.6H_2O$, KOH, H_2SO_4(95-98wt%) and ethyl alcohol were bought from Sigma-Aldrich Chemical Reagent Co.

Preparation of PBMC and PBMO

PBMC was prepared as follows. In a typical synthesis, in order to remove the oil, a piece of NF was immersed in ethyl alcohol at room temperature for 2 min. Then NF was dipped into 5 volume% H_2SO_4 for 2min at room temperature to remove the oxide of NF surface. Then NF was immersed into 5g/L phytic acid (PA) solution for 1h at room temperature. Finally, NF was immersed into 50g/L $FeCl_3.6H_2O$ solution for 1h at room temperature. It is noting that NF will be cleaned by deionized water for several times among the above two processes. To obtain PBMO by electrochemical oxidization process, such PBMC was electrochemical oxidized with a scan rate of 5 mV/s at the region from +0 to +0.8 V versus Hg/HgO in 1.0 M KOH electrolyte.

Some reaction equations during the fabrication process are shown in **scheme S1**.

Characterizations

The morphology of samples was observed by ZEISS SEM Supra 40. Transmission electron microscopy (TEM) of samples was carried out on a JEOL-3010 (300 kV acceleration voltage). XRD patterns were measured by Bruker D8 Advanced

Diffractometer System. The element analysis of samples was determined by X-ray photoelectron spectroscopy (XPS, Kratos AXIS Ultra DLD). The Fourier transform infrared (FT-IR) spectra and Raman spectra were conducted on a Varian 3100 Excalibur Series FT-IR Spectrophotometer and a Horiba MicroRaman HR Evolution System, respectively.

Electrochemical measurements

OER were studied in a typical three-electrode cell connected to a Bio-logic VMP 3 using the PBMO/NF as the working electrode($1\times1 cm^2$), Pt as a counter electrode and Hg/HgO as a reference electrode. All the measured potentials were converted to reversible hydrogen electrodes (RHE) according to $E(RHE)=E_{Hg/HgO}+0.059\ pH+0.098$ V. LSV curves were carried out with the scan rates of 1mV/s. Tafel slopes of the experiments were all derived from LSV curves. EIS was measured under the following conditions: frequency ranges 200 kHz to 100 mHz. All the electrochemical datas were presented with 100% iR conpensation.

(1) Self-assembly process

I chelation reaction

$$\mathrm{Ni+PA} \longrightarrow \mathrm{Ni^{2+}\text{-}Phytate+H_2}\uparrow$$

II absorption reaction

$$\mathrm{Ni^{2+}\text{-}Phytate+PA} \longrightarrow \mathrm{Ni^{2+}\text{-}Phytate\text{-}PA}$$

(2) Etching-Catching process

I etching reaction

$$\mathrm{Ni+2Fe^{3+}} \longrightarrow \mathrm{Ni^{2+}+2Fe^{2+}}$$

II catching reaction

$$\mathrm{Ni^{2+}\text{-}Phytate\text{-}PA+Ni^{2+}+Fe^{3+}+Fe^{2+}} \longrightarrow \mathrm{Ni^{2+}\text{-}Fe^{3+}\text{-}Fe^{2+}\text{-}Phytate}$$

III absorption reaction

$$\mathrm{Ni^{2+}\text{-}Fe^{3+}\text{-}Fe^{2+}\text{-}Phytate+pCl^{-}} \longrightarrow \underset{\textbf{PBMC}}{\mathrm{Ni^{2+}\text{-}Fe^{3+}\text{-}Fe^{2+}\text{-}Phytate\text{-}Cl_p}}$$

(3) Electrochemical Oxidization process

electrochemical oxidation reaction

$$\mathrm{Ni^{2+}\text{-}Fe^{3+}\text{-}Fe^{2+}\text{-}Phytate\text{-}Cl_p+mKOH\text{-}ne^{-}} \longrightarrow \underset{\textbf{PBMO}}{\mathrm{NiO(OH)\text{-}FeO_t(OH)_c\text{-}Phytate\text{-}K_mCl_p}}$$

Note:

$\mathrm{NiO(OH)\text{-}FeO_t(OH)_c\text{-}Phytate\text{-}K_mCl_p}$ can also be marked as $\mathrm{NiO(OH)K_aCl_b\text{-}FeO_t(OH)_cK_xCl_y\text{-}Phytate}$

Scheme S1 Some reaction equations during the fabrication process

Supplementary Explanation

The explanation of redox reaction of Ni and Fe^{3+}

$$\mathrm{Ni^{2+}+2e^{-} \rightleftharpoons Ni(s)} \quad \mathbf{E^{\ominus}= -0.25V} \qquad \mathbf{(1)}$$

$$\mathrm{Fe^{3+}+e^{-} \rightleftharpoons Fe^{2+}} \quad \mathbf{E^{\ominus}= 0.77V} \qquad \mathbf{(2)}$$

$$\Delta G^{\ominus} = -nF\Delta E^{\ominus} \qquad \mathbf{(3)}$$

$$\Delta E^{\ominus} = 2 * 0.77 - (-0.25) = 1.79 > 0.2V \qquad (4)$$

$\Delta E^{\ominus} > 0 \; so \; \Delta G^{\ominus} < 0$

According to Rule of experience, when $\mathbf{\Delta E^{\ominus}} > 0.2V$, Redox reaction can be carried out automatically.

So Ni can reacts with Fe^{3+} according to the below equation:

$$\mathrm{Ni+2Fe^{3}}(5) \longrightarrow \mathrm{Ni^{2+}+2Fe^{2+}}$$

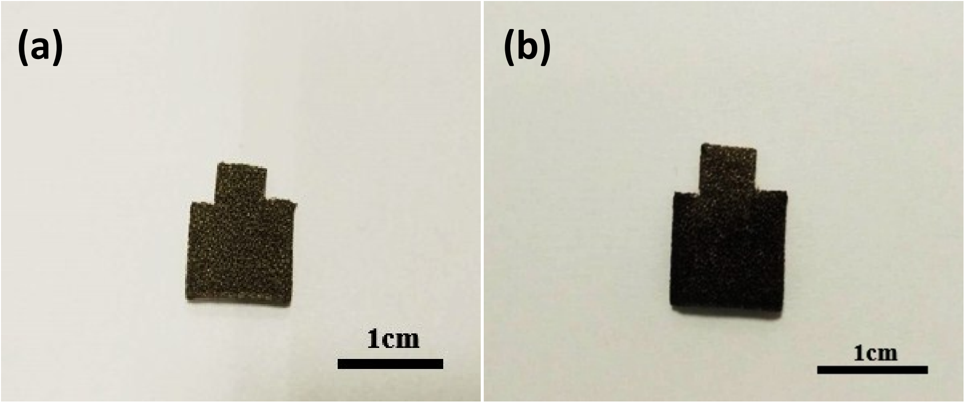

Figure S1 the digital photos of PBMC(a) and PBMO(b)

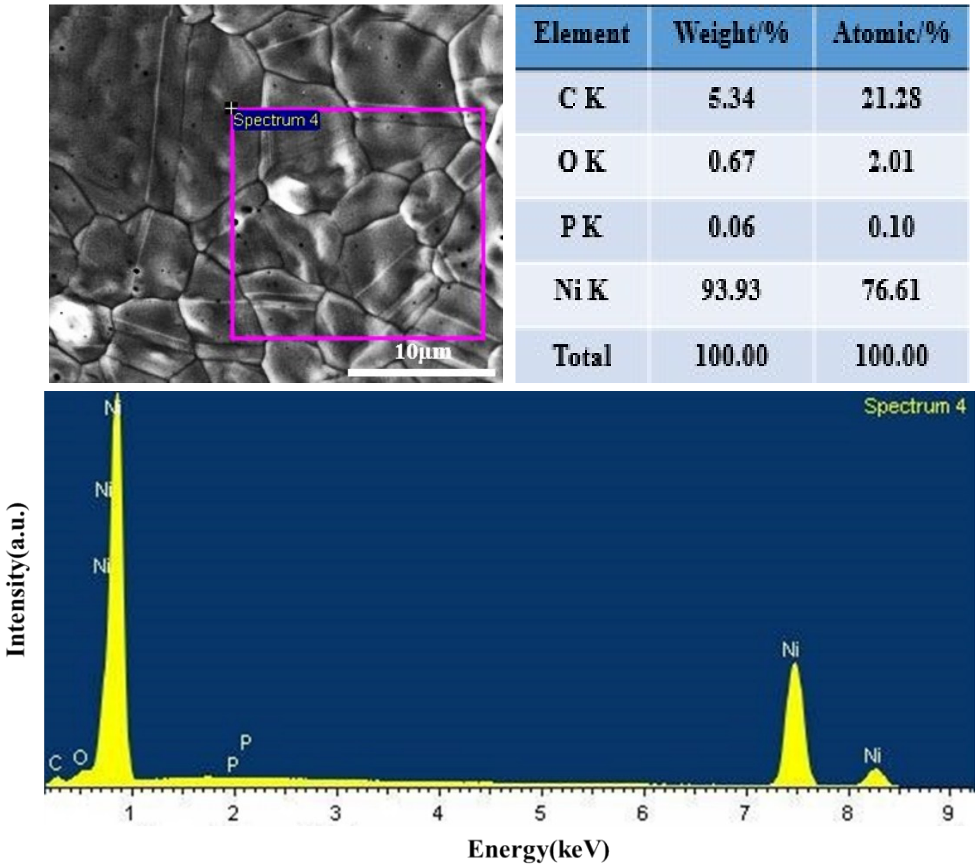

Element	Weight/%	Atomic/%
C K	5.34	21.28
O K	0.67	2.01
P K	0.06	0.10
Ni K	93.93	76.61
Total	100.00	100.00

Figure S2 EDS test image and test results after self-assembly process

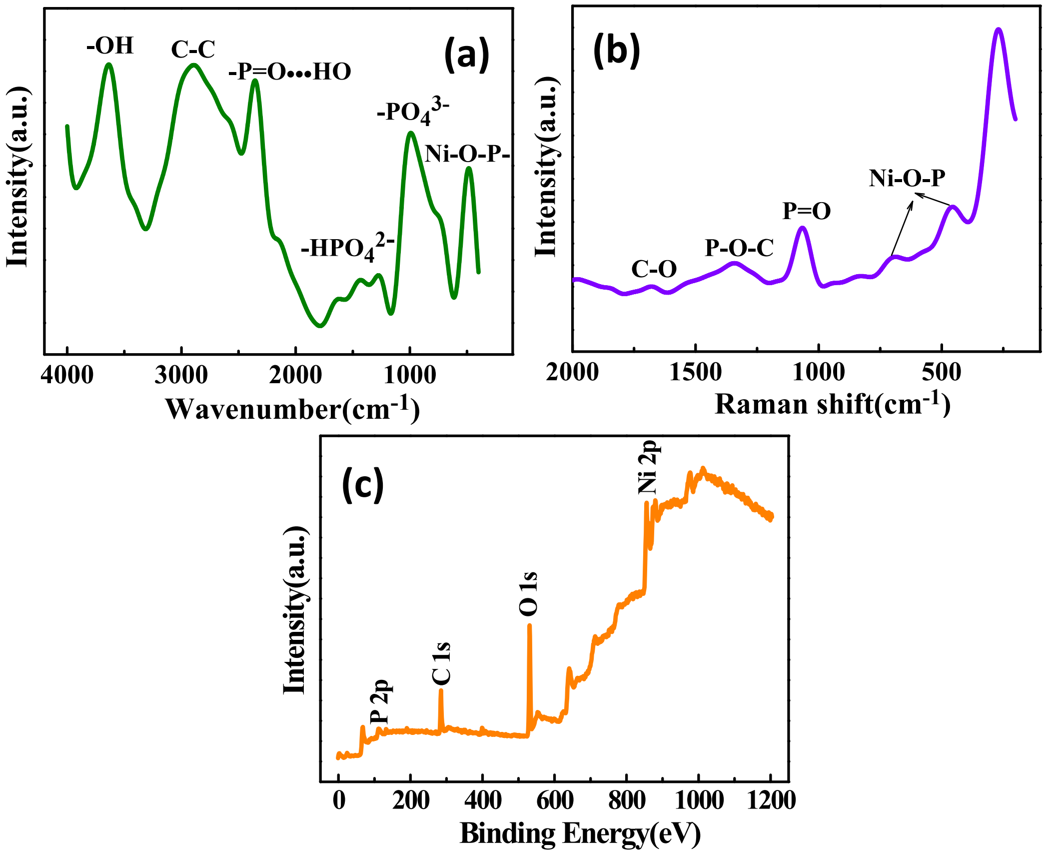

Figure S3 The spectroscopic characterization of nickel foam after self-assembly process (a) FTIR spectra of nickel foam after self-assembly process (b) Raman spectra of nickel foam after self-assembly process (c) XPS spectra of nickel foam after self-assembly process

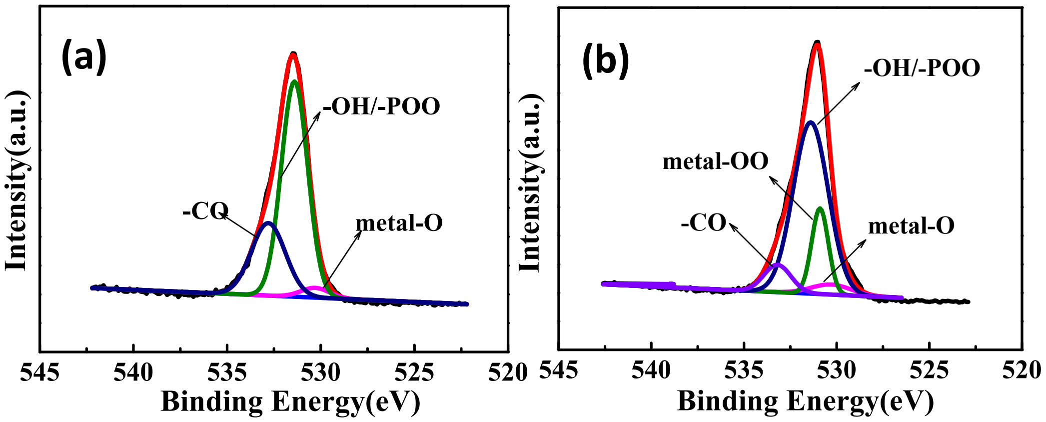

Figure S4 (a) The XPS spectrum of O element of PBMC (b) The XPS spectrum of O element of PBMO

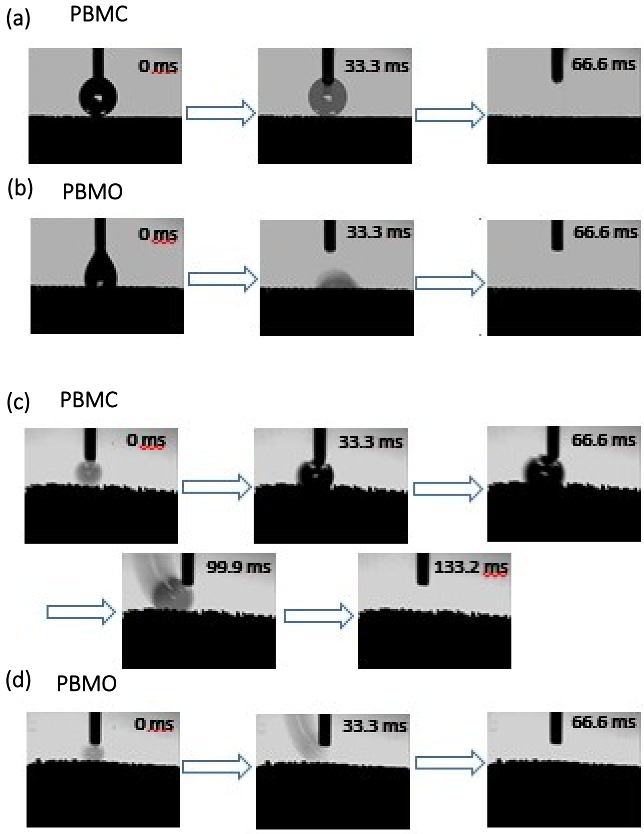

Figure S5 The dynamic hydrophilicity and aerophobicity property of as-prepared materials. (a) the water droplet wetting process observation of PBMC. (c) the water droplet wetting process observation of PBMO. (c) the air bubble wetting process observation underwater of PBMC (d) the air bubble wetting process observation underwater of PBMO.

Note: The contact angle instrument use stainless steel as needle and the alkali droplet can not be dropped smoothly owing to “Alkali climbing” phenomenon. Herein, the dynamic wetting process of as-prepared materials in alkali solution(1M KOH) can not be observed. The contact angle data of the alkali droplet(1M KOH) wetting property of different materials were obtained by using manual plastic needle.

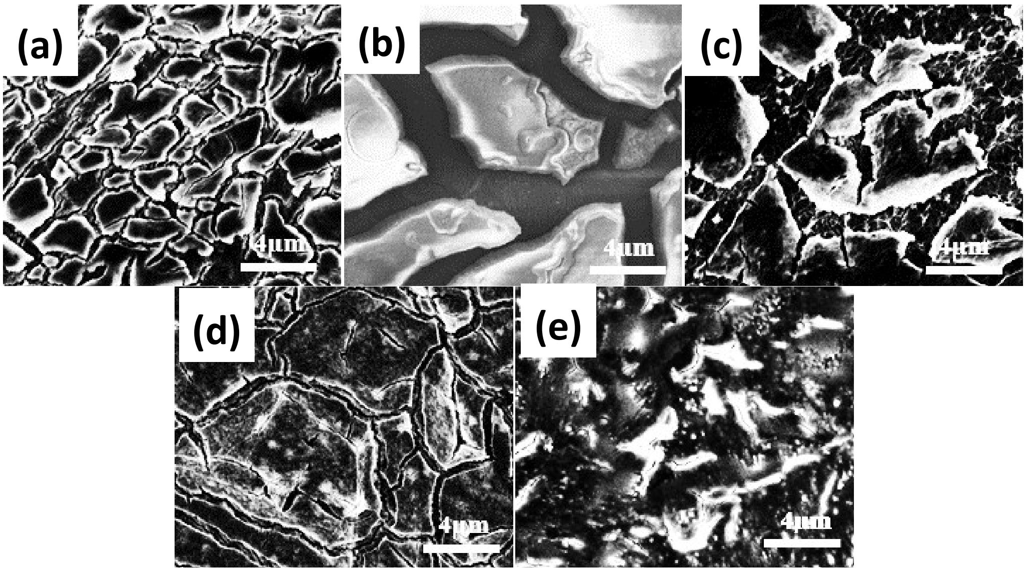

Figure S6 The influence of different etching-catching time on the morphology of PBMC (a) 0.5h (b) 1h (c) 1.5h (d) 2h (e) 2.5h

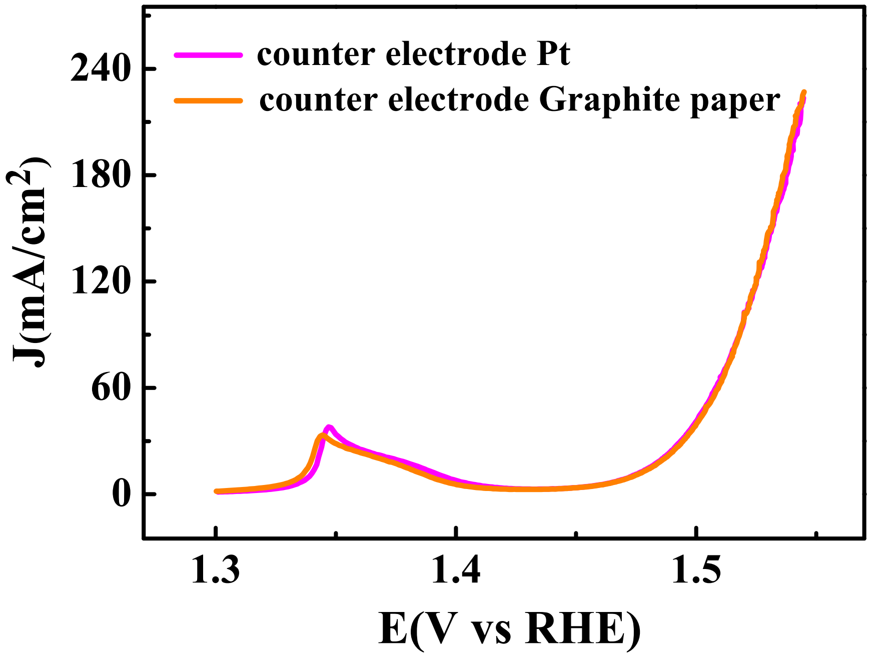

Figure S7 The LSV performance of PBMO under different counter electrode.

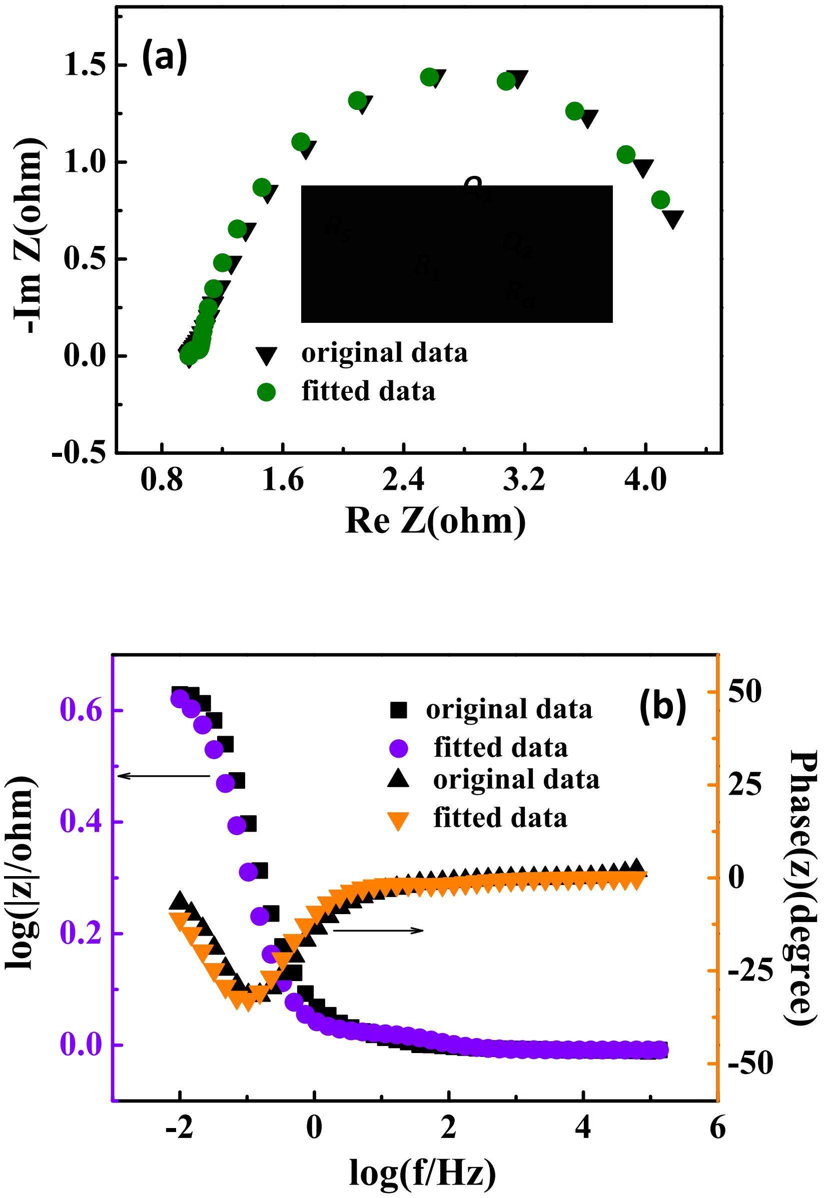

Figure S8 EIS(a) and Bode curves(b) of PBMO at 1.48V vs RHE.

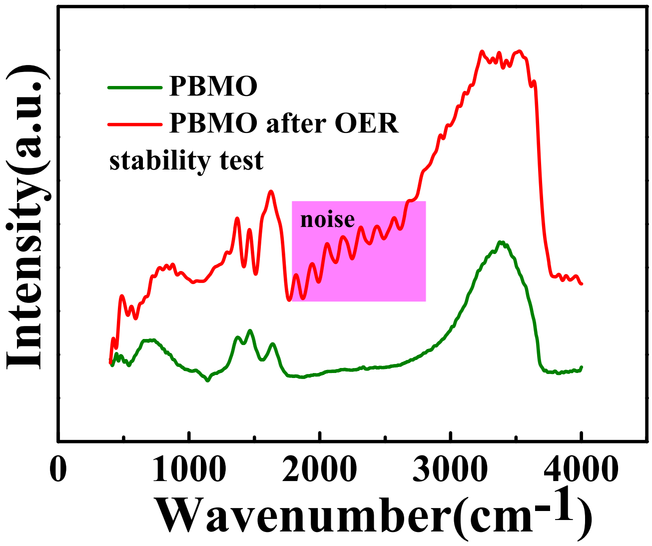

Figure S9 FTIR of PBMO and PBMO after OER stability test.

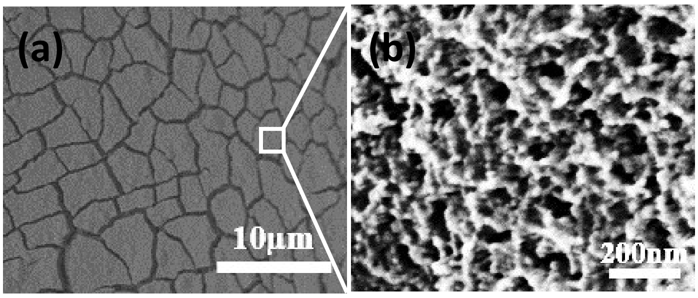

Figure S10 SEM image(a) and magnification SEM image(b) of PBMO after OER stability test

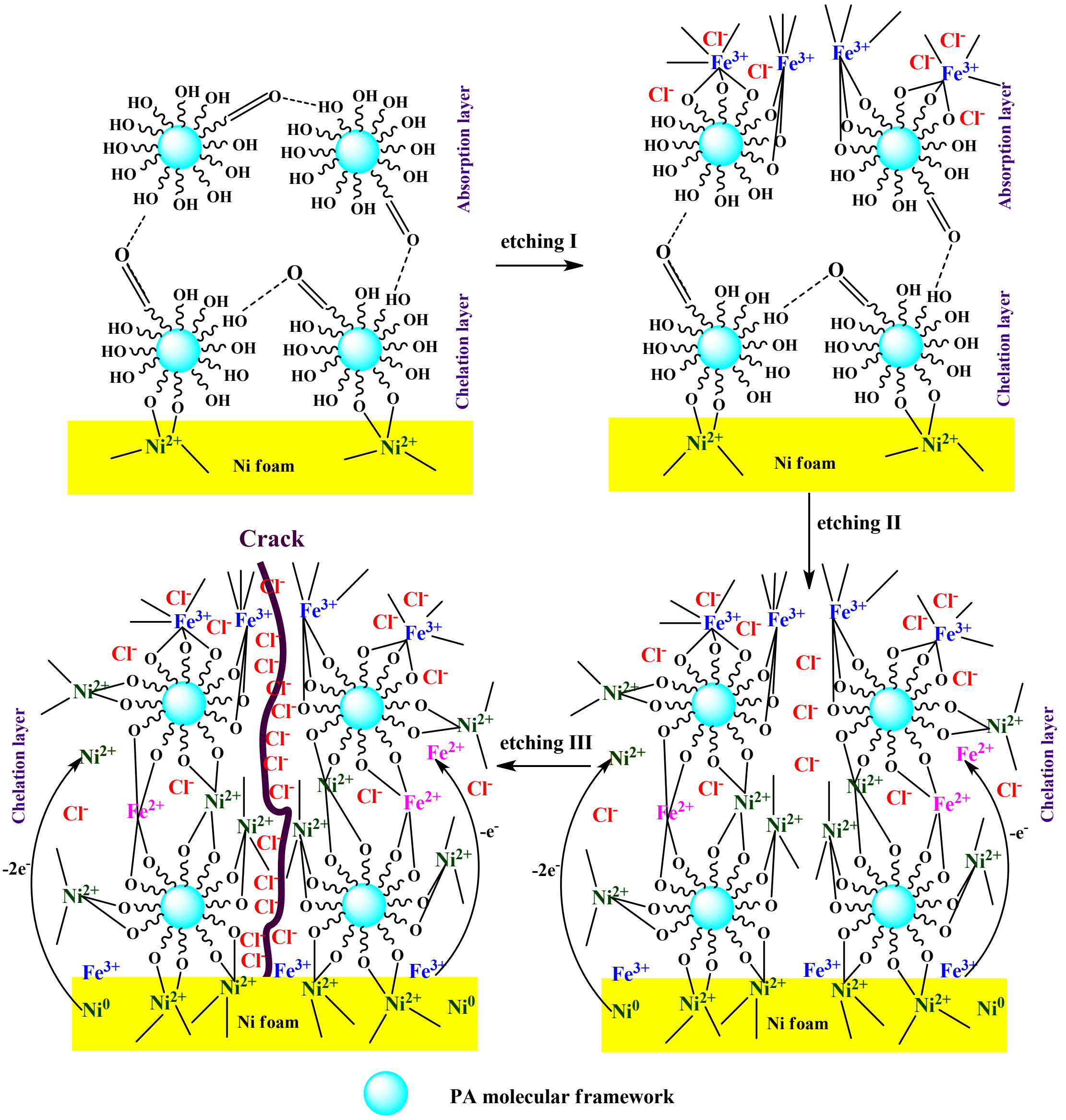

Scheme S2 the formation process of island-shaped PBMC template

Scheme S2 can interpret the formation process of PBMC. When Ni foam after self-assembly was immersed into $FeCl_3$ solution, PA molecular in absorption outside layer can chelate Fe^{3+} during etching I period. With the extension of time, the redox corrosion reaction generates more and more metal ion and abundant metal ion is chelated by PA molecular, and the PA layer turns to the complete chelation layer. At the same time, some Cl^- penetrate into the gap with PA-metal complex molecular(etching II period). With prolonging the time, more and more pitting corrosion even stress corrosion crack phenomenon appears. Moreover, Cl$^-$ can absorb inside of PBMC by absorption effect. Finally, PBMC template with enriched nanopores and microcrack diffusion tunnels is formed on Ni foam.

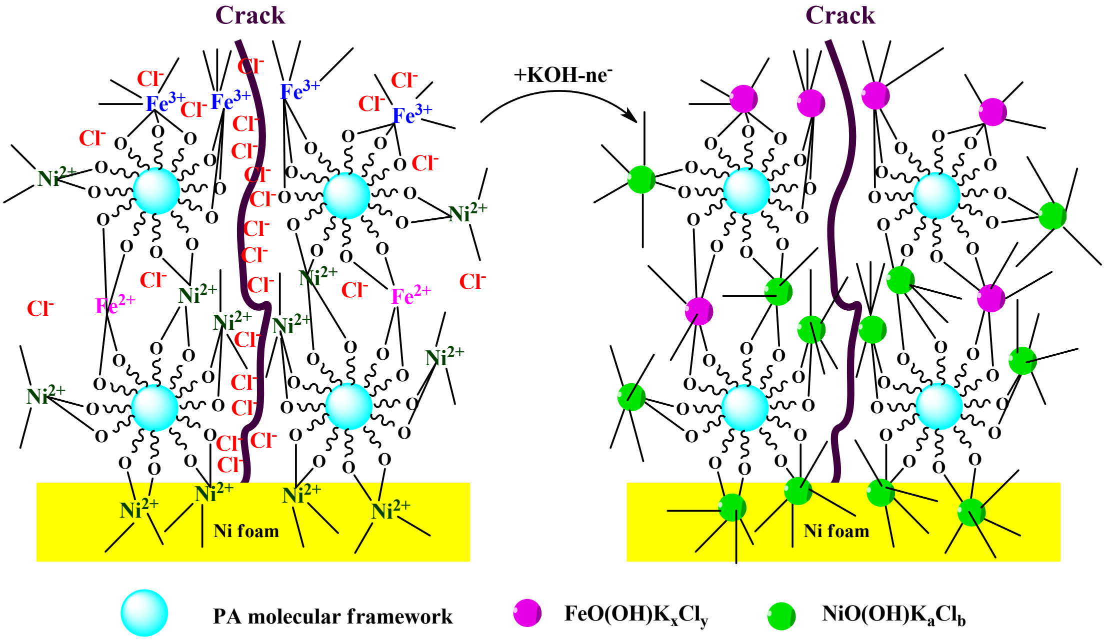

Scheme S3 the formation process of PBMO during anodization process.

Scheme S3 can describe the formation process of PBMO. Firstly, the metal site of PBMC is electrochemically oxidized to nanosphere phytate-metal oxyhydroxide. Secondly, K$^+$ can be doped into PBMO by electrochemical and chemical oxidation corrosion reaction. At last, PBMO in situ grows on Ni foam.

Table S1. ICP test of electrolyte before and after OER stability test(10mA/cm^2, 10h)

Electrolyte	Ni/ppm	Fe/ppm
Before OER stability test	ND	0.02
After OER stability test	ND	<0.01

Note: ND means “Not Detected”.

Supplementary METHODS

Calculation of $ECAS$ (electrochemically active surface area)

The electrochemical double-layer capacitance C_{dl} is calculated as the below equation:

$$C_{dl} = J_c \div v \quad \textbf{(1)}$$

The charge current J_c was measured from CV curves where no apparent Faradaic process happened. v is the scan rate as shown in **Fig 4j**.

As shown in **Fig 4k**, the electrochemical double-layer capacitance C_{dl} value of PBMO is 9.54 mF.

The electrochemically active surface area $ECAS$ is calculated as the below equation according to the previous reports:

$$ECAS = C_{dl} \div C_s \quad \textbf{(2)}$$

The specific capacitance value of the sample C_s is 0.040 mF/cm^2 according to the literatures, so the $ECAS$ of PBMO/NF electrode is 238.5cm^2.

Calculation of RF (roughness factor)

The roughness factor RF of as-prepared PBMO/NF electrode is 238.5 as determined by the below equation 3:

$$RF = ECAS \div GSA \quad \textbf{(3)}$$

The geometric surface area (GSA) of the PBMO/NF electrode is 1cm^2.

Table S2. Summary of the electrocatalytic OER activity of the previously reported NiFe-based catalysts in 1M KOH electrolyte

Catalyst	*j* [mA /cm^2]	Overpotential [mV] @*j*	Tafel slope (mV /dec)	Substrate	Ref
PBMO	10	243	44	NF	This work
	20	256			
	100	290			
Ni-MOF@Fe-MOF	10	265	82	GCE	*Adv. Funct. Mater., 2018, 1801554*
NiFe LDHUF	10	254	32	Graphite paper	*Adv. Energy Mater., 2018, 1703585*
HG-NiFe	10	310	39	GCE	*Sci. Adv., 2018, 4.*
Fe_3O_4/Ni_xP	10	260	43	GC-RDE	*ACS Energy Lett., 2018, 3, 141.*
Fe-Ni@NC-CNTs	10	274	45.47	GCE	*Angew. Chem. Int. Ed., 2018,57,8921*
	100	322			
NiFe LDH/CNTs	10	~250	31	GCE	*J. Am. Chem. Soc.,* 2013, *135*, 8452.
$Ni_{0.75}Fe_{0.25}Se_2$ hollow nanochains	10	267	67	GCE	*Nano Energy, 2018, 47, 275.*
FeNi-LDH/Ti_3C_2-MXene	20	258	48	NF	*Nano Energy, 2018, 44, 181.*
$Ni_{2/3}Fe_{1/3}$ LDH nanosheets	10	310	76	GCE	*ACS Nano,* 2015, *9*, 1977.
NiFe LDH-NS	10	300	40	GCE	*Nat. Commun.,* 2014, *5*, 4477.
NiFe LDH	10	280	47.6	HOPG	*J. Am. Chem. Soc.,* 2014, *136*, 13118
	100	363			
Fe/(Ni)OOH	10	290	32	SS	*Angew. Chem. Int. Ed.,* 2016, *55*, 9937.
$Ni_{1.5}Fe_{0.5}P$	10	264	55	GCE	*Nano Energy, 2017,* 34, 472.
	20	280	55	GCE	
	100	293	114	CF	

Table S3. Summary of the electrocatalytic OER activity of as- reported organic metal-based and organic metal-derived catalysts in 1M KOH electrolyte

Catalyst	j [mA /cm^2]	Overpotential [mV] @ j	Tafel slope (mV /dec)	Substrate	Ref
PBMO	10	243	44	NF	This work
	20	256			
	100	290			
Ni-MOF@Fe-MOF	10	265	82	GCE	*Adv. Funct. Mater., 2018, 1801554*
Co-PBA-plasma-2h	10	274	53	NF	*Adv. Energy Mater., 2018, 1800085*
NiFe-UMNs	10	260	30	GCE	*Nano Energy, 2018, 44, 345.*
MAF-X27-OH	10	387	60	GCE	*J. Am. Chem. Soc., 2016, 138, 8336.*
MAF-X27-OH/Cu foil	10	338	82	Cu Foil	
CoOx-ZIF	10	318	70.3	GCE	*Adv. Funct. Mater., 2017, 1702546.*
P-doped-Co@NC-3/1	10	340	85	GCE	*Adv. Energy Mater., 2018, 8, 1702048*
NiCo@NiCoO$_2$/C PMRAs	20	366	83.97	carbon fabric	*Adv. Mater., 2018, 30, 1705442*
Co$_3$O$_4$/Co-Fe DSNBs	10	297	61	GCE	*Adv. Mater., 2018, 1801211.*
Co3Ni3(bdc)4(OH)4	10	189	-	CF	*Nat Energy, 2016, 1, 16184*
Hierarchically structured Co3O4@CoP	10	238	51.4	Ni foil	*Adv. Energy Mater., 2017, 7, 1602643*
Fe-Ni@NC-CNTs	10	274	45.47	GCE	*Angew. Chem. Int. Ed., 2018,57,8921*
	100	322			
IrO2/C(52 wt%)	10	250	87	GCE	*J. Am. Chem. Soc., 2014, 136, 13925.*

GCE: glassy carbon electrode,
NF: nickel foam
CF: copper foam

Au-RDE: Au rotating disk electrode,
HOPG: highly-ordered pyrolytic graphite,
SS: stainless steel

REFERENCES

1. K. Rui, G. Q. Zhao, Y. P. Chen, Y. Lin, Q. Zhou, J. Y. Chen, J. X. Zhu, W. P. Sun, W. Huang and S. X. Dou, *Adv. Funct. Mater.*, 2018, **1801554**.
2. X. Zhao, P. Pachfule, S. Li, J. R. J. Simke, J. Schmidt and A. Thomas, *Angew. Chem. Int. Ed.*, 2018, **57**, 8921.
3. Y. Guo, T. Wang, J. Chen, J. Zheng, X. Li and K. Ostrikov, *Adv. Energy Mater.*, 2018, **1800085**.
4. G. Hai, X. Jia, K. Zhang, X. Liu, Z. Wu and G. Wang, *Nano Energy.*, 2018, **44**, 345.
5. X. -F. Lu, P. -Q. Liao, J. -W. Wang, J. -X. Wu, X. -W. Chen, C. -T. He, J. -P. Zhang, G. -R. Li and X. -M. Chen, *J. Am. Chem. Soc.*, 2016, **138**, 8336.
6. S. Dou, C. -L. Dong, Z. Hu, Y.-C. Huang, J. -l. Chen, L. Tao, D. Yan, D. Chen, S. Shen, S. Chou and S. Wang, *Adv. Funct. Mater.* 2017, **27**, 1702546.
7. Y. Li, B. Jia, Y. Fan, K. Zhu, G. Li and C.-Y. Su, *Adv. Energy Mater.*, 2018, **8**, 1702048.
8. H. Xu, Z. -X. Shi, Y. -X. Tong and G. -R. Li, *Adv. Mater.,* 2018, **30**, 1705442.
9. X. Wang, L. Yu, B. Y. Guan, S. Song and X. W. Lou, *Adv. Mater.*, 2018, **1801211**.
10. J. Zhou, Y. B. Dou, A. Zhou, R. M. Guo, M. J. Zhao and J. R. Li, *Adv. Energy Mater.*, 2017, **7**, 1602643.
11. S. Zhao, Y. Wang, J. Dong, C. -T. He, H. Yin, P. An, K. Zhao, X. Zhang, C. Gao, L. Zhang, J. Lv, J. Wang, J. Zhang, A. M. Khattak, N. A. Khan, Z. Wei, J. Zhang, S. Liu, H. Zhao and Z. Tang, *Nat Energy*, 2016, **1**, 16184.
12. T.Y. Ma, S. Dai, M. Jaroniec and S.Z. Qiao, *J. Am. Chem. Soc.*, 2014, **136**, 13925.
13. Y. Zhao, X. Zhang, X. Jia, G. I. N. Waterhouse, R. Shi, X. R. Zhang, F. Zhan, Y. Tao, L. -Z. Wu, C. -H. Tung, D. O'Hare and T. Zhang, *Adv. Energy Mater.,* 2018, **1703585**.

14. J. Wang, L. Gan, W. Zhang, Y. Peng, H. Yu, Q. Yan, X. Xia and X. Wang, *Sci. Adv.*,2018, **4**.
15. A. Dutta, S. Mutyala, A. K. Samantara, S. Bera, B. K.Jena and N. Pradhan, *ACS Energy Lett.* 2018, **3**, 141.
16. M. Gong, Y. Li, H. Wang, Y. Liang, J. Z. Wu, J. Zhou, J. Wang, T. Regier, F. Wei, and H. Dai, *J. Am. Chem. Soc.,* 2013, **135**, 8452.
17. Lin. L, Z. Li, K.-H. Xue, Y. Ruan, X. Ao, H. Wan, X. Miao, B. Zhang, J. Jiang, C. Wang and K. (K.) Ostrikovef, *Nano Energy.*, 2018, **47**, 275.
18. M. Yu, S. Zhou, Z. Wang, J. Zhao and J. Qiu, *Nano Energy.*, 2018, **44**, 181.
19. W. Ma, R. Ma, C. Wang, J. Liang, X. Liu, K. Zhou and T. Sasaki, *ACS Nano*, 2015, **9**, 1977.
20. F. Song and X. Hu, *Nat. Commun.,* 2014, **5**, 4477.
21. B. M. Hunter, J. D. Blakemore, M. Deimund, H. B. Gray, J. R. Winkler and A. M. Müller, *J. Am. Chem. Soc.*, 2014, **136**, 13118.
22. H. Zhong, J. Wang, F. Meng and X. Zhang, *Angew. Chem. Int. Ed.,* 2016, **55**, 9937.
23. H. Huang, C. Yu,C. Zhao, X. Han, J. Yang, Z. Liu, S. Li, M. Zhang and J. Qiu, *Nano Energy.*, 2017, **34**, 472.